Journal of Alloys and Compounds 512 (2012) 328–331

Contents lists available at SciVerse ScienceDirect

Journal of Alloys and Compounds

journal homepage: www.elsevier.com/locate/jallcom

Microstructure development in laser forming of zirconium coatings on AZ91D magnesium alloy substrates

T.M. Yue[a,*], H. Xie[a], X. Lin[a], H.O. Yang[b]

[a] The Advanced Manufacturing Technology Research Centre, Department of Industrial and Systems Engineering, Hong Kong Polytechnic University, Hung Hom, Hong Kong
[b] State Key Laboratory of Solidification Processing, Northwestern Polytechnical University, Xi'an, PR China

ARTICLE INFO

Article history:
Received 29 April 2011
Received in revised form
24 September 2011
Accepted 29 September 2011
Available online 8 October 2011

Keywords:
Laser forming
Zirconium
Coating
Magnesium
Solidification
Microstructure

ABSTRACT

Zr-coatings were fabricated on AZ91D magnesium alloy substrates using laser forming by means of a blow powder technique. Multi-passes were required to form a pure Zr top coating layer on the AZ91D Mg substrate. The microstructure and phases of the coating were studied using XRD, EDS and SEM. The alloy element Al in AZ91 alloy was found to be important for the formation of a metallurgically bonded interface between the Zr coating and the matrix material. The coating can be classified as a three-layer structure with a pure Zr layer at the top surface. The development of the coating microstructure is explained with the aid of a schematic solidification scheme.

1. Introduction

In the study of biomechanics, more and more attention has been paid to the stress transmission condition between hard tissue and biomaterials, from the point of view of bone resorption. A problem with currently used metallic implants is that they are very much stiffer than bone, so they shield the nearby bone from mechanical stresses. Stress shielding results in a type of disuse atrophy, bone resorbs, and subsequently loosening of the implant occurs. The modulus of cortical bone varies and is also dependent on orientation. Typical values are between 10 and 30 GPa [1], which are many times lower than most of the currently used metallic implant materials.

Examining the existing commercially available metals and alloys, it is not difficult to realise that Mg is probably the most appropriate metal that can fulfil the density and stiffness requirements best. Indeed, as early as 1907, magnesium was reported as having been used to secure a fracture in a human leg [2]; Mg is also an important element of biomaterials [3]. Although the attempt failed, as the metal corroded too rapidly, interest in using Mg for orthopaedic implants has not gone cold but remains strong. In fact, in recent years, there has been a strong interest in exploring the use of Mg and its alloys as degradable biomaterials. This is largely due to the test results which found that the corrosion rate of Mg and its alloys, when tested in physiological environments, can be modulated through the use of high purity Mg, or new alloying systems and surface treatments [4,5]. On the other hand, it is considered that if the corrosion problem of Mg can be resolved, Mg or its alloys can be considered to be good candidates for long-term implantation applications.

Among the many surface modification methods, laser surface treatment [6–12], including laser cladding has been used successfully to deposit different coating materials on Mg and its alloys in order to improve their corrosion and wear resistance. With regard to laser cladding of Zr on Mg, the early work of Subramanian et al. [6] on the laser cladding of Mg–Zr alloys on Mg substrates showed that an excellent metallurgical bond was obtained. However, the research work did not consider the effects of alloying elements on the formation of the interfacial bond. Moreover, multi-layer cladding conditions, which are often required for forming a relatively thick corrosion and wear resistant coating, have not been considered. Recognizing this, the present research addressed the issue on alloying elements and studied the microstructure development under multi-layer cladding conditions. This research also aims to laser form a pure Zr coating on Mg with a good metallurgically bonded interface, and this has not been reported in the literature. Zr was employed because the metal and its oxides display excellent electrochemical properties and biocompatibility [13,14].

The approach of this research was to explore the use of the laser forming technique to fabricate a new type of Mg–Zr biomaterials

* Corresponding author. Fax: +852 23625267.
E-mail address: mftmyue@inet.polyu.edu.hk (T.M. Yue).

0925-8388/$ – see front matter © 2011 Elsevier B.V. All rights reserved.
doi:10.1016/j.jallcom.2011.09.091

of which the core material to be Mg which has a relatively low Young's modulus. On top of the magnesium core, a layer of Zr is fabricated. It is envisaged that owing to the low density of Mg and the excellent corrosion resistance and biocompatibility of Zr, the requirements for long-term applications can be satisfied. Thus, if laser forming of Mg–Zr materials is successfully developed, it would provide the orthopaedic implant industry with a promising alternative method to produce high-performance artificial biomaterials. This paper forms part of a wider study that investigates laser forming of graded Zr coatings on Mg substrates, and focuses on studying microstructure development.

2. Experimental

Laser forming was performed using a 4 kW continuous wave CO_2 laser from Prima North America Inc., equipped with a four-axis numerical control working table and a lateral powder feeder nozzle. The laser powder and focus spot size were set at 1.5 kW and 3 mm, respectively, while a scanning rate of 10 mm/s was used. The experiment was conducted inside a controlled-atmosphere glove box, where high-purity argon gas was continuously supplied at a flow rate of 10 l/min during the experiment to prevent the molten metal from oxidizing. Zr powder was deposited and re-melted on the AZ91D (Mg–9Al–1Zn) magnesium alloy substrate, of surface area 40 mm × 40 mm. The coating powder was 99.2 wt.% pure Zr with a mesh size of 300–320. Prior to the deposition experiment, the Zr powder was dried in a vacuum oven for 24 h. The Zr metal powder was delivered into the laser processing zone using a lateral powder feeder, with the aid of an argon gas jet. The feed angle between the substrate and the powder feeder nozzle was 60°. In the experiment, the focus point of the laser beam was adjusted to a position slightly above the substrate surface so as to melt the Zr powder before it reached the surface. This arrangement was necessary because the melting point of Zr (2125 K) is much higher than the boiling point of Mg (1380 K). In order to create a coating, multi-tracks were produced, with an overlapping percentage of 30%, and the coating was formed by the deposition of four layers of Zr powder. The total thickness of the coating was about 2 mm. The specimens for microscopic study were ground with various sized of emery paper and then polished with 1 μm diamond abrasives. The microstructure of the material was revealed using a JEOL scanning electron microscope equipped with energy dispersive X-ray spectroscopy (EDX). The specimens were in the unetched condition.

3. Results and discussion

3.1. Microstructural examination

Fig. 1 presents the backscattered images of the cross-section microstructure of a Zr-coated specimen. For ease of discussion, the coating can be divided into three layers, i.e., a top Zr layer with a thickness of approximately 1 mm (A in Fig. 1a), below which is a narrow band of matrix material (B in Fig. 1a), and further towards the substrate is a composite layer containing Zr particles in the matrix material (C in Fig. 1a). These figures also reveal that a Zr coating that is free from major defects can be formed on the AZ91 substrate with a metallurgically bonded interface. A closer examination of the top Zr layer shows that it is actually made up of two zones, as delineated by the dashed line (Fig. 1b). According to the results of a series of EDS analyses (Fig. 2) performed across the lower part of the top Zr layer and band B (Fig. 1b), the upper zone was confirmed to be of primarily zirconium, while the lower zone consists of elements of Zr and Al. The EDS results also show that there was a continuous change of Zr and Al content in the lower zone. It is interesting to note that in the lower zone, a relatively high Al content was detected without the presence of Mg.

3.2. Microstructure development of the laser formed coating

Fig. 3 shows a schematic sketch describing the development of the microstructure during laser rapid forming of the Zr coating on an AZ91D magnesium alloy substrate under a multi-pass condition. In the laser deposition of the first pass, i.e., the first layer, the laser energy was largely absorbed by the Mg substrate and resulted in a shallow melt pool, into which the Zr particles were fed. Upon solidification, a composite layer containing Zr particles in an AZ91 matrix was obtained (region D in Fig. 3). During laser deposition of the second pass, part of zone D, which consists of Zr particles in the AZ91 matrix, was re-melted, i.e., region M. Since liquid Mg and liquid Zr are not miscible, Mg will not mix with Zr, however Al of AZ91 will diffuse into the liquid Zr. As a result, a relatively low melting point liquid, rich in Zr with Al, is produced, and is separated from

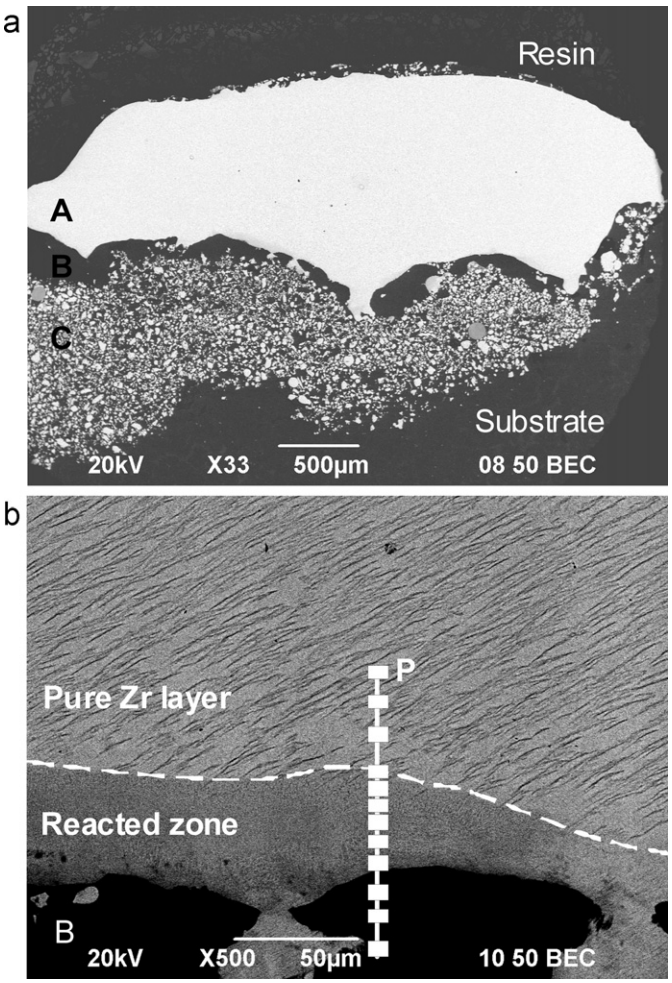

Fig. 1. (a) An overall image of the Zr coating, (b) an enlargement of an area towards the bottom of layer A, showing the reacted zone.

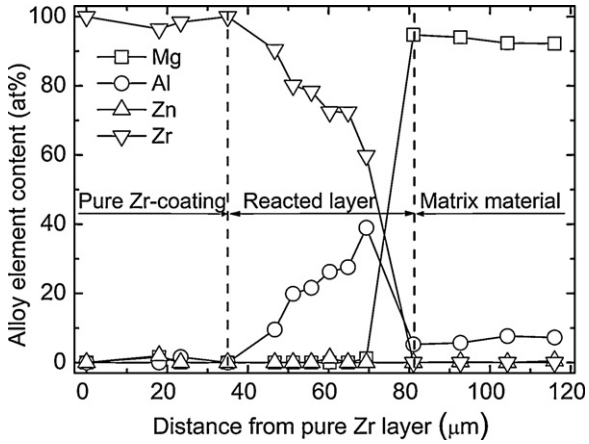

Fig. 2. Elements distribution across the Zr coating as a function of distance from point P, as labelled in Fig. 1b.

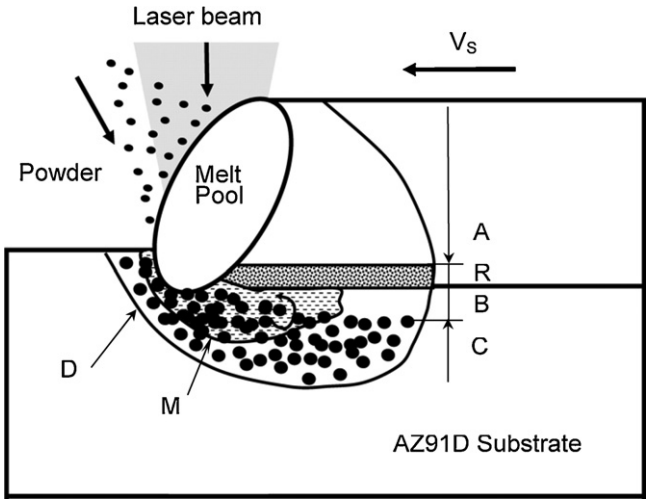

Fig. 3. A schematic diagram showing the different layers developed during laser rapid forming, where A is pure Zr, R is the reacted zone, B is the matrix material, and C consists of Zr particles in the AZ91 matrix.

the melt of the matrix (region B). The relatively low melting point Zr–Al liquid formed is trapped between the solidifying Zr layer on the top (A) and the liquid Mg pool (B) underneath, and subsequently forms the reacted zone (R) as the solidification continues. It is also evident that a few Zr particles in region M were not totally melted and finally became part of the reacted zone (Fig. 4).

To further analyse the solidification behaviour of the reacted zone, a XRD pattern was obtained for an area of the reacted zone (Fig. 5). However, since the detection spot (about 0.8 mm) was actually larger than the zone itself, the XRD pattern obtained also revealed the solid solution (Mg) phase which originated from layer B (Fig. 1). In addition to the diffraction peaks of (Zr) and (Mg), the peaks for Zr_4Al_3 and Zr_3Al_2 phases are also revealed; and there was no ternary phase found. Moreover, the $Mg_{17}Al_{12}$ phase found in the XRD pattern of the AZ91D substrate (insert in Fig. 5) was not detected. Based on the XRD results, it is clear that the Al element in an AZ91 alloy plays an important role in forming a reacted zone which metallurgically bonds the matrix material and the top Zr layer. Considering the conditions of rapid solidification during laser deposition, only a relatively short time is available for the development of the reacted zone, therefore, its thickness is relatively small of about 50 μm. A magnification of the microstructure at the interface between the top Zr layer and the reacted zone, shown in Fig. 6, reveals that the Zr rich dendrites appear in white, while the

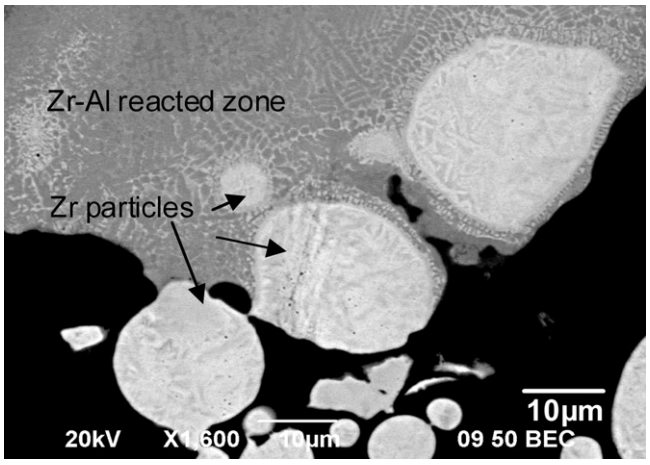

Fig. 4. Un-melted zirconium particles adhering to the bottom of the reacted zone.

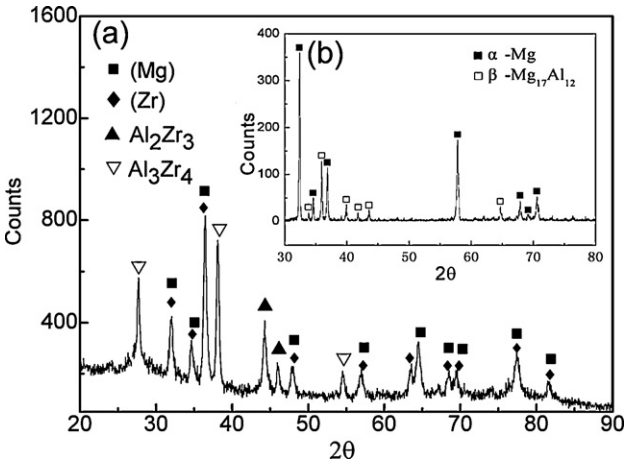

Fig. 5. An XRD pattern obtained for an area of the reacted zone; insert (b) showing the XRD pattern obtained for the AZ91D substrate.

compounds of Zr_4Al_3 and Zr_3Al_2, are in dark grey. The former was growing from the bottom of the Zr layer in a direction towards the substrate over a distance of about 5–10 μm. Such a backward cellular growth phenomenon in laser deposition has been reported by the author previously [15], and was attributed to the presence of a relatively low melting point liquid phase existing at the substrate interface, and the situation is similar to the present case.

It should be pointed out that based on the Zr–Al equilibrium phase diagram (Fig. 7), a series of phase evolutions occur when Al is increased from zero to 40 at.% that would result in the formation of solid solution (Zr), Zr_3Al, Zr_2Al, Zr_3Al_2, and Zr_4Al_3 compounds. However, it is interesting to note that in the reacted zone, only (Zr), Zr_3Al_2 and Zr_4Al_3 were found, and there was no evidence of the presence of Zr_3Al and Zr_2Al. According to the Zr–Al phase diagram (Fig. 7), Zr_2Al and Zr_3Al are products of two peritectoid reactions: $\beta(Zr) + Zr_5Al_3 \rightarrow Zr_2Al$ and $\beta(Zr) + Zr_2Al \rightarrow Zr_3Al$, respectively. Since sufficient time is required for solid diffusion to occur, in order to complete the peritectoid reactions, it is likely that the formation of Zr_3Al and Zr_2Al was suppressed due to the rapid cooling conditions of the laser forming process. As for Zr_3Al_2 and Zr_4Al_3, which are the decomposition products of high temperature phases of Zr_5Al_3 and Zr_5Al_4, there is only a small composition difference between them, and the transformations could occur more easily due to reheating under the multi-pass laser forming condition.

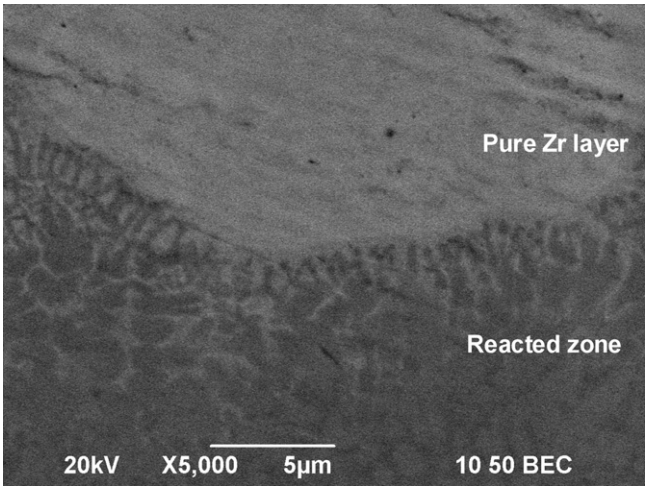

Fig. 6. A backscattered image of the microstructure of the interface between the top Zr layer and the reacted zone.

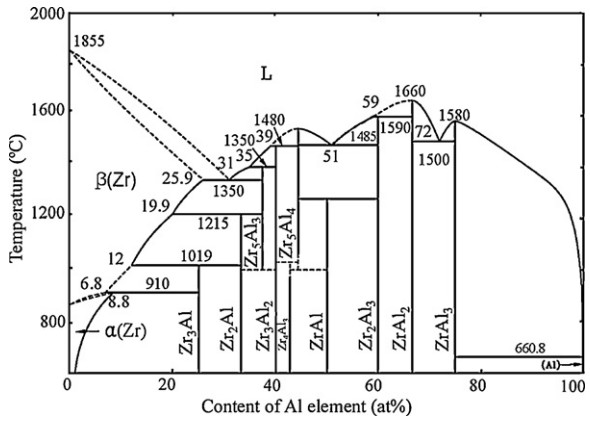

Fig. 7. Al–Zr binary equilibrium phase diagram [16].

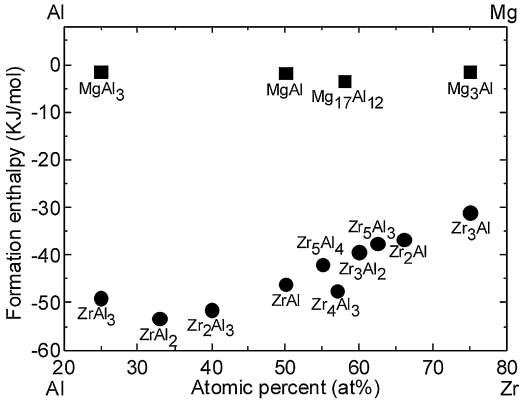

Fig. 8. Heat of formation as a function of alloy composition for the Al–Zr and Al–Mg systems, with data from [17] and [18], respectively.

The formation of Zr–Al intermetallics in the reacted zone is essentially a result of a competing process between the phase formation of the Al–Zr and Mg–Zr systems. Fig. 8 shows the heat of formation for various intermetallics of the Al–Zr system. Relatively large negative values of the heat of formation were obtained for the compounds of the Al–Zr system, indicating that they can be formed readily. Moreover, a literature review of the Mg–Zr system revealed that there was virtually no reaction between these two elements. Furthermore, with the limited solubility of Mg in Zr, and a high affinity of Al to Zr, the chance of forming $Mg_{17}Al_{12}$ phase in the reacted zone would be small. It is considered that even though there may be a small amount of Mg in the reacted zone, the $Mg_{17}Al_{12}$ phase would not form, since its heat of formation is less negative than those of the Al–Zr compounds (Fig. 8).

4. Conclusions

Pure Zr-coatings were successfully fabricated on AZ91D magnesium substrates using the laser multi-pass deposition technique. The study showed that a metallurgical bond was formed at the interface between the coating and the matrix material, and it is considered that Al played an important role in the formation of the metallurgical bond. Moreover, the microstructure of the coating can be categorized into a three-layer structure. Starting from the surface is a pure Zr layer, below which lies an Zr–Al reacted zone. Next is a layer of matrix material and finally a layer consisting of a composite of Zr particles in the matrix material. Intermetallics, Zr_4Al_3 and Zr_3Al_2 were found in the reacted layer, and their formation is due to the strong affinity of Al to Zr. However, due to the rapid solidification conditions in laser forming, the equilibrium phases of Zr_3Al and Zr_2Al were not found in the reacted zone.

Acknowledgements

The work described in this paper was fully supported by a grant from the Research Grants Council of the Hong Kong Special Administrative Region, China (Project No. PolyU 534508). The authors would also like to thank the Hong Kong Polytechnic University and the Northwestern Polytechnical University for providing the research facilities.

References

[1] K.-H. Kramer, in: H. Stallforth, P. Revell (Eds.), Materials for Medical Engineering, Wiley/VCH Verlag GmbH, Weinheim, 2000, pp. 9–29.
[2] A. Lambotte, Bull. Mém. Soc. Nat. Chir. 28 (1932) 1325–1334.
[3] V. Rodriguez-Lugo, G.A. Camacho-Bragado, V.M. Castano, Mater. Manuf. Processes 8 (1) (2003) 67–78.
[4] F. Witte, F. Feyerabend, P. Maier, J. Fischer, M. Stormer, C. Blawert, W. Dietzel, N. Hort, Biomaterials 8 (13) (2007) 2163–2174.
[5] E. Zhang, L.P. Xu, K. Yang, Scripta Mater. 3 (5) (2005) 523–527.
[6] R. Subramanian, S. Sircar, J. Mazumder, J. Mater. Sci. 26 (1991) 951–956.
[7] T. Maiwald, R. Galun, B.L. Mordike, F.J. Feikus, Laser Eng. 2 (4) (2002) 227–238.
[8] T.M. Yue, Y.P. Su, J. Mater. Sci. 42 (15) (2007) 6153–6160.
[9] C.S. Wang, T. Li, B.A. Yao, R. Wang, C.A. Dong, Surf. Coat. Technol. 205 (1) (2010) 189–194.
[10] M. Qian, D. Li, S.B. Liu, S.L. Gong, Corros. Sci. 2 (10) (2010) 3554–3560.
[11] W. Khalfaoui, E. Valerio, J.E. Masse, M. Autric, Opt. Lasers Eng. 8 (9) (2010) 926–931.
[12] X. Cao, M. Xiao, M. Jahazi, J. Fournier, M. Alain, Mater. Manuf. Processes 23 (3–4) (2008) 413–418.
[13] Y. Tsutsumi, D. Nishimura, H. Doi, N. Nomura, T. Hanawa, Acta Biomater. 6 (10) (2010) 4161–4166.
[14] Y. Han, Y.Y. Yan, C.G. Lu, Y.M. Zhang, K.W. Xu, J. Biomed. Mater. Res. A 88 (1) (2009) 117–127.
[15] T.M. Yue, T. Li, Mater. Trans. 8 (5) (2007) 1064–1069.
[16] H. Okamoto, J. Phase Equilib. 4 (2) (1993) 257–259.
[17] G. Ghosh, M. Asta, Acta Mater. 53 (2005) 3225–3252.
[18] X.Y. Liu, P.P. Ohotnicky, J.B. Adams, C.L. Rohrer, R.W. Hyland, Surf. Sci. 373 (1997) 357–370.